THE JOURNAL OF PHYSICAL CHEMISTRY C

Article

pubs.acs.org/JPCC

Rate of Molecular Exchange through the Membranes of Ionic Liquid Filled Polymersomes Dispersed in Water

Soonyong So[†] and Timothy P. Lodge*[,†,‡]

[†]Department of Chemical Engineering & Materials Science and [‡]Department of Chemistry, University of Minnesota, Minneapolis, Minnesota 55455, United States

Supporting Information

ABSTRACT: The permeation of 1-ethyl-3-methylimidazolium ([EMIM]), 1-butyl-3-methylimidazolium ([BMIM]), and 1-butylimidazole through the bilayer membranes of nanoemulsion-like polymersomes was investigated by nuclear magnetic resonance spectroscopy (NMR) techniques. 1,2-Polybutadiene-*b*-poly(ethylene oxide) (PB−PEO) polymersomes in the ionic liquid (IL) 1-ethyl-3-methylimidazolium bis-(trifluoromethylsulfonyl)imide ([EMIM][TFSI]) were prepared by a cosolvent method and then migrated to the aqueous phase, which is not miscible with the IL, at room temperature. In this way stable, nanoscopic domains of the IL (average diameter ca. 200 nm) were dispersed in water. Two similarly sized molecules, charged [EMIM] and neutral 1-butylimidazole, were employed as tracer molecules, and proton NMR (^{1}H NMR) and pulsed-field-gradient NMR (PFG-NMR) experiments were conducted. Furthermore, transient ^{1}H NMR was used with [BMIM] to estimate how rapidly the charged molecules can go through the hydrophobic membrane into the polymersome interior. The molecules in the nanoemulsion solution showed two distinct sets of peaks due to the magnetic susceptibility difference across the membrane. This difference in ^{1}H NMR gave direct evidence of permeation of the molecules and the relative populations within the polymersomes versus in the aqueous exterior. The escape and entry rates were evaluated by fitting the PEG-NMR echo decay curves with a two-site exchange model. The molecules could permeate through the hydrophobic PB membranes on a time scale of seconds, but the entry and escape rates for the charged molecule ([EMIM]) were approximately 10 times slower than the neutral molecule (1-butylimidazole). These results confirm that this system has the potential to serve as a nanoreactor, facilitating reactions with various kinds of molecules including both charged and neutral molecules. It combines the facile transport and mixing of a majority aqueous phase with the multiple advantages of IL as a reaction medium. The ability to shuttle the polymersomes reversibly between aqueous and ionic liquid phases offers a convenient route to product separation and catalyst recovery.

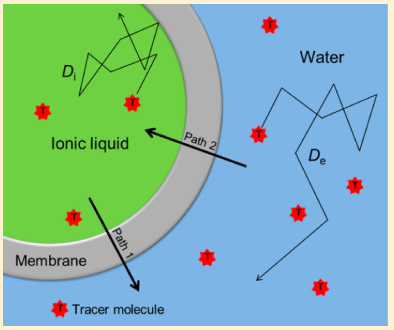

INTRODUCTION

Polymeric vesicles prepared from amphiphilic block copolymers, or polymersomes, have attracted increased attention as potential "nanoreactors" due to tunability of their building blocks and similarity to biological cell structures. Vesicles exhibit both confined interiors and membranes that provide enough room to load active substances.[1] For example, the internal space of vesicles can be used to encapsulate and deliver active materials, e.g., fragrances, drugs, catalysts, and reactants.[2−4] The use of vesicles in such applications depends on their membrane properties (e.g., permeability and stability), which can be controlled and tuned by precise molecular design of the constituting blocks.[5] In this regard, polymersomes have greater flexibility and versatility via readily tuned parameters such as block length and chemical structure, compared to liposomes prepared from low molecular weight phospholipids.[6]

Recently, Bai and Lodge developed a new kind of polymersome solution or "nanoemulsion", in which a water-immiscible ionic liquid (IL) is compartmentalized within water.[7] The vesicle bilayers comprised poly(butadiene-*b*-ethylene oxide) (PB−PEO) diblock copolymers, and contained 1-ethyl-3-methylimidazolium bis(trifluoromethylsulfonyl)-imide) [EMIM][TFSI]. The IL-filled polymersomes are distinct from canonical vesicles, which have the same fluid inside and outside.[1,6,8] They offer an opportunity to design new reaction processes by installing appropriate catalysts within the IL interiors, while maintaining the facile molecular transport, low viscosity, and cost-effectiveness of an aqueous majority phase.[9,10] These vesicles are prepared via a thermoresponsive polymersome "shuttling" in the biphasic system of water and IL. After transfer of the polymersomes from a hydrophobic IL to water, the IL inside the polymersomes remains segregated and stabilized from the aqueous phase by the hydrophobic and IL-phobic bilayer PB core.[11]

This reversible shuttle of the IL-filled polymersomes exhibits characteristics of both homogeneous and heterogeneous catalysis. Since the locus of the reaction is the liquid interior of the polymersomes, the reaction is potentially homogeneous, yet this system resembles heterogeneous catalysis in that facile and quantitative recovery of the polymersome nanoreactors and

Received: May 24, 2014
Revised: August 19, 2014
Published: August 28, 2014

catalyst can be conducted via the reverse thermoresponsive shuttle. The properties of such nanoemulsion-like polymersomes have not been studied extensively, and particularly the rate of molecular transfer into and out of the polymersomes has not been characterized; clearly the rate of molecular transport across the membrane will be an important factor in any reaction system design.[12] Especially, when polymersomes have completely different phases across the membranes, the permeability has not been explored. The change of chemical potential for a reagent or product molecule at each interface (IL−membrane or water−membrane) is not the same, in contrast to conventional vesicles, which have symmetric interfaces across the membrane. The permeation rate can be affected by the partitioning of a probe molecule between the two fluids in addition to the solubility and diffusivity of the probe molecules in the membrane, and the time scale of molecular permeation for each direction needs to be understood to optimize the system for nanoreactor applications.

Quantification of permeability is not straightforward compared to conventional polymersome systems. Previous studies of vesicle permeation have employed fluorescence or UV−vis spectroscopy. Through these methods, the amount of molecules released from the vesicles or loaded to the vesicles can be quantified, and the permeability can be obtained. However, there are limitations in the selection of permeants in order to use either fluorescence or UV−vis spectroscopy.[13−21] In particular, tracer molecules should have partition coefficients between vesicle interior and exterior fluids on the order of unity. In this study, the molecular exchange of small molecules through the bilayer membranes is investigated by a combination of ^{1}H NMR spectroscopy and pulsed-field-gradient (PFG-NMR) techniques. NMR is a powerful tool because any molecule having an NMR-active nucleus can be used.[22−24] In the nanoemulsion solution, tracer molecules exhibit two diffusion coefficients in the two different environments and are exchanged across the membranes between two immiscible phases. Two similarly sized probes, [EMIM] and 1-butylimidazole, were used in order to quantify the permeation through the hydrophobic membranes. As far as we are aware, this is the first example that resolves molecular permeation into and out of the polymersomes separately. The results demonstrate a powerful tool to analyze molecular transport in nanoemulsion-like polymersome solutions, whereby it is possible to quantify the rates of reagent entry and product escape from an IL-filled nanorector.

EXPERIMENTAL SECTION

Materials. A 1,2-polybutadiene-*b*-poly(ethylene oxide) (PB−PEO) block copolymer was synthesized via sequential anionic polymerization by adding ethylene oxide to ω-hydroxyl 1,2-polybutadiene homopolymer (PB-OH). First, the PB-OH was synthesized in anhydrous tetrahydrofuran (THF) at −60 °C with *sec*-butyllithium as initiator. The polymerization was capped by addition of one ethylene oxide unit and then terminated by adding deoxygenated methanol. Characterization by ^{1}H NMR spectroscopy and size exclusion chromatography (SEC) gave a number-average molecular weight (M_n) and dispersity ($Đ$) of 9.3 kg/mol and 1.04, respectively. The synthesized PB-OH was dissolved in anhydrous THF and converted into macroinitiator using diphenylmethyl potassium as an electron transfer agent. Weighed ethylene oxide was added to the reactor at room temperature, and the temperature was increased to 45 °C. After 24 h, the reaction was terminated in the same manner as PB-OH. The polymer was characterized by ^{1}H NMR spectroscopy and SEC to obtain M_n and $Đ$, as summarized in Table 1. The synthesized PB−PEO was designated BO(9−3) based on the M_n of the PB and PEO blocks (9.3 and 2.5 kDa, respectively). [EMIM][TFSI] was synthesized by combining equal moles of 1-ethyl-3-methylimidazolium bromide ([EMIM][Br], Io-Li-Tec, 99%) and lithium bis(trifluoromethylsulfonyl)imide ([Li][TFSI], HQ115) with water, as described previously.[25] 1-Butylimidazole (98%) and 1-butyl-3-methylimidazolium chloride ([BMIM]Cl, 99%) were purchased from Aldrich and Io-Li-Tec, respectively, and used as received.

Table 1. Characteristics of Polymer and Vesicles with [EMIM][TFSI] Interiors Dispersed in D_2O

polymer	M_{PB}[a] (kg/mol)	M_{PEO}[b] (kg/mol)	$Đ$[c]	$\langle R_h \rangle$[d] (nm)	μ_2/Γ^2[e]
BO(9−3)	9.3	2.5	1.07	64	0.1

[a]Number-average molecular weight of the ω-hydroxylpoly(butadiene) homopolymer (PB-OH) determined by ^{1}H NMR spectroscopy. The fraction of 1,2-addition was 91%. [b]Number-average molecular weight of PEO block obtained from ^{1}H NMR spectroscopy and the PB-OH molecular weight. [c]Dispersity (M_w/M_n) of PB−PEO determined by SEC. [d]Average hydrodynamic radius. [e]Dispersity of polymersomes determined by DLS.

Polymersome Solution Preparation. The polymersomes were prepared through a cosolvent method to obtain a narrow size distribution. BO(9−3) was first dissolved in dichloromethane, and then an equal mass of [EMIM][TFSI] was added. The solution was dried by N_2 purge to selectively remove dichloromethane. Vesicle formation was prompted by slow evaporation of the dichloromethane to yield a 0.5 wt % polymersome solution in nonvolatile [EMIM][TFSI]. The polymersomes with IL interiors were then allowed to migrate from the IL solution to an immiscible aqueous phase. A weighed amount of deuterium oxide (D_2O) was added to the [EMIM][TFSI] solution of polymersomes according to the target polymersome content in D_2O (0.5, 1.0, or 1.5 wt %). The polymersomes transferred to the aqueous phase at room temperature with stirring (∼100 rpm). The two immiscible phases were in contact for at least 12 h at room temperature to allow complete transfer. After the transfer, the ionic liquid phase on the bottom turned clear, and the upper aqueous phase became cloudy due to light scattering from the vesicles. The cloudy aqueous phase was then carefully removed for the NMR studies. The size and dispersity of the prepared polymersomes were measured by dynamic light scattering (DLS). For the exchange of [EMIM], the aqueous solution was used as prepared ($C_{[EMIM]} \sim 42$ mM, which was calculated by using the solubility of [EMIM][TFSI] in water[26] and the volume of the polymersomes). For 1-butylimidazole and [BMIM] studies, 50 mM of 1-butylimidazole or [BMIM]Cl was added to the aqueous polymersome dispersion, respectively, and the solution was stirred for at least 1 day to allow equilibration.

NMR Measurements. A Bruker Avance III 500 MHz NMR spectrometer equipped with a 5 mm triple resonance broad band PFG probe was used for both ^{1}H NMR spectroscopy and pulsed-field-gradient NMR (PFG-NMR) at 25 °C. All PFG-NMR measurements were conducted on ^{1}H nuclei with DOSY (diffusion-ordered spectroscopy), using the "ledbpgp2s" pulse sequence (longitudinal eddy current delay experiment using bipolar gradients acquired in 2D mode).[27] Two gradient pulses

dx.doi.org/10.1021/jp505118h | J. Phys. Chem. C 2014, 118, 21140−21147

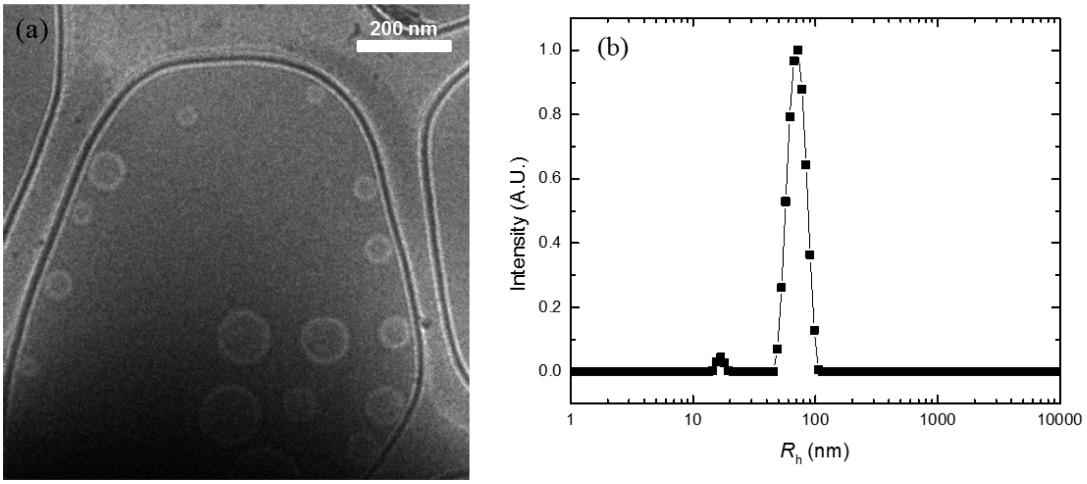

Figure 1. (a) Cryo-TEM images of 0.5 wt % BO(9−3) polymersomes in [EMIM][TFSI] (scale bar: 200 nm). (b) Normalized hydrodynamic radius (R_h) distribution of 0.01 wt % BO(9−3) polymersomes in [EMIM][TFSI].

with a strength G (ranging from 2% to 98% of the maximum gradient strength, 0.47 T/m) were applied for a duration (δ) in the pulse sequence. The intensity attenuation (I) of probe molecules with the gradient strength variation was recorded during a diffusion time (Δ) and processed by the Top Spin software package (version 3.1) in order to extract the translation diffusion coefficient (D). In the presence of free diffusion of probe molecules, the intensity (I) is attenuated with respect to the intensity (I_0) at $G = 0$ as

$$\frac{I}{I_0} = \exp(-\gamma^2\delta^2G^2D(\Delta - \delta/3)) \quad (1)$$

where γ is the proton gyromagnetic ratio (42.6 MHz/T). D can be evaluated from the slope of the linear plot of $\ln(I/I_0)$ vs $(-\gamma^2\delta^2G^2(\Delta - \delta/3))$.

Cryogenic Transmission Electron Microscopy (Cryo-TEM). The nanostructure of BO(9−3) in [EMIM][TFSI] was analyzed by cryo-TEM. Specimens were prepared in a FEI Vitrobot Mark III vitrification robot. In the climate chamber of the Vitrobot, 0.5 μL of the polymersome solution (0.5 wt %) was loaded onto a carbon-coated and lacey film-supported copper TEM grid, and then the grid was plunged into liquid ethane (∼−180 °C). The rapidly cooled samples were kept in liquid N_2 before measurements. Cryo-TEM imaging was performed using a FEI Tecnai G2 Spirit BioTWIN operating at 120 kV under liquid N_2 cryo conditions, and the images were taken with an Eagle 4 megapixel CCD camera. All images were obtained at an underfocus for adequate phase contrast (Figure 1a).

Dynamic Light Scattering (DLS). DLS was performed over a range of angles (60°−120°) with a Brookhaven BI-200SM goniometer and a Brookhaven BI-9000AT correlator at λ = 637 nm and 25 °C to obtain the average hydrodynamic radius $\langle R_h \rangle$. The dispersity of particle size was quantified by the reduced second cumulant μ_2/Γ^2. The mean decay rate ($\Gamma = D_m q^2$, where D_m is the mutual diffusion coefficient and q is the scattering vector) and the μ_2 values were obtained from cumulant fitting of the normalized correlation function (see Figure S1). The polymersome size distribution (Figure 1b) was also assessed through the Laplace inversion routine, REPES.[28] For the DLS measurement, polymersome solutions in [EMIM][TFSI] were diluted to 0.01 wt % by adding filtered [EMIM][TFSI] through a syringe filter (Millex-SV 5.0 μm).

RESULTS AND DISCUSSION

Polymersome Characterization. A vesicle structure was observed in the ionic liquid solution of BO(9−3), consistent

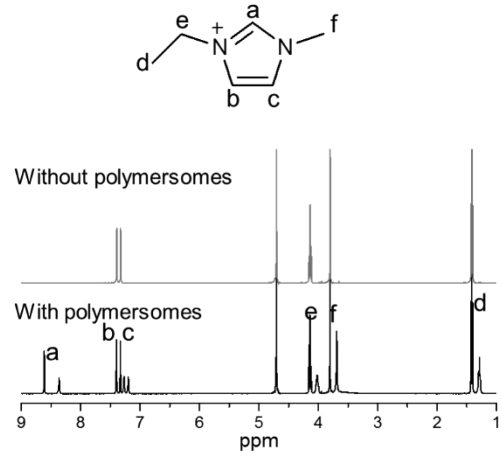

Figure 2. Chemical structure of [EMIM] and ^{1}H NMR spectrum of [EMIM] without and with BO(9−3) polymersomes (solvent peak at 4.7 ppm).

with previous PB−PEO block copolymers with low volume fractions of PEO (∼0.2).[7,18,29,30] Polymersomes with mean radius less than 100 nm and narrowly dispersed in size are shown in the cryo-TEM image (Figure 1a). Relatively monodisperse small polymersomes were obtained using a volatile organic cosolvent, which can dissolve both PB and PEO blocks, and is miscible with the ionic liquid. The circular bright regions represent the PB membranes and appear brighter than the IL matrix due to lower electron density, while the solvated PEO corona is invisible in the medium. Because both [EMIM][TFSI] and water are selective solvents for PB−PEO, and PEO shows a change in affinity with temperature in the biphasic system of [EMIM][TFSI] and water, upon adding D_2O (or water) to the IL solution at room temperature, the polymersomes moved spontaneously from the IL phase to the aqueous phase while retaining the vesicle structure and the IL interiors. Even after the transfer from the IL phase to the aqueous phase, the PB−PEO polymersomes retained their structure and size (see Figure S2), as reported previously.[7]

dx.doi.org/10.1021/jp505118h | J. Phys. Chem. C 2014, 118, 21140−21147

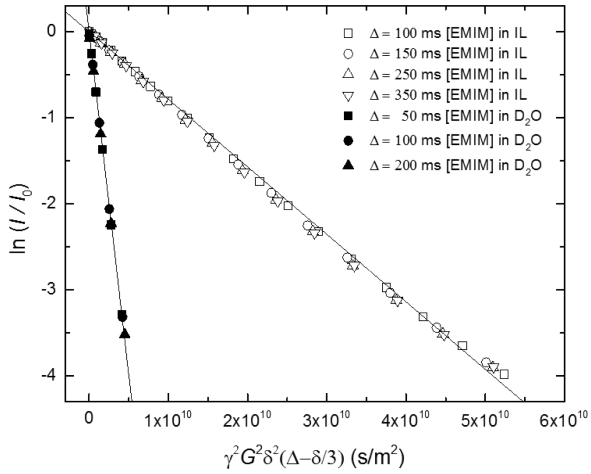

Figure 3. Echo decay curves of [EMIM] in D_2O and [EMIM][TFSI] with variation of the field gradient strength G for different diffusion times Δ with δ = 8 ms.

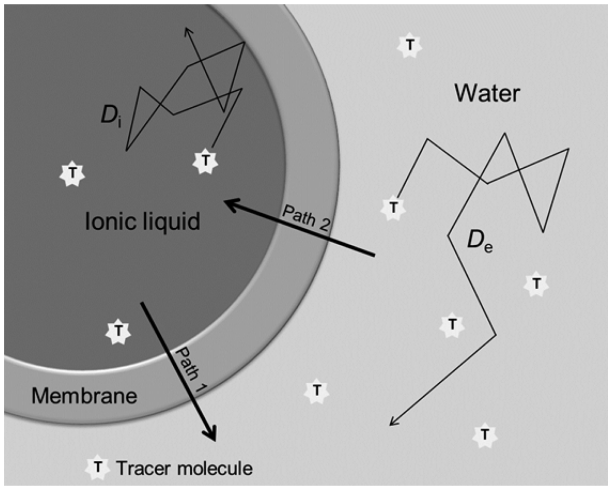

Figure 4. Schematic of molecular diffusion in each phase and transportation across the membrane of polymersome with IL interior dispersed in water. The tracer molecules move with diffusion coefficient D_i inside and D_e outside of the polymersomes. Also, the molecules are exchangeable across the membranes through path 1 and path 2.

BO(9−3) polymersomes have essentially the same membrane thickness before and after the transfer, 21 ± 2 and 22 ± 2 nm, respectively, as measured by ImageJ software. This membrane thickness lies on the scaling line of $d \sim N^{0.6}$ of the membrane thickness of various PB−PEO vesicles in water, where d is the membrane thickness and N is the degree of polymerization.[31] The size and dispersity of polymersomes in the ionic liquid were analyzed by DLS, and the mean hydrodynamic radius $\langle R_h \rangle$ = 67 nm with dispersity μ_2/Γ^2 = 0.13.

Equilibrium Partitioning of Imidazole Derivatives in Polymersome Solutions. ^{1}H NMR spectra of [EMIM]-[TFSI] in D_2O ([EMIM][TFSI] saturated), and in the polymersome solution, were measured in order to see the effect of polymersomes on the chemical shift of [EMIM] (Figure 2). The solution without polymersomes shows a single set of distinct peaks of [EMIM] protons in D_2O. (The signal for proton H_a was not observed due to hydrogen−deuterium exchange.[32]) The single peak around 4.7 ppm arises from protons of ^{1}HDO and ^1H_2O in D_2O. However, [EMIM] in the

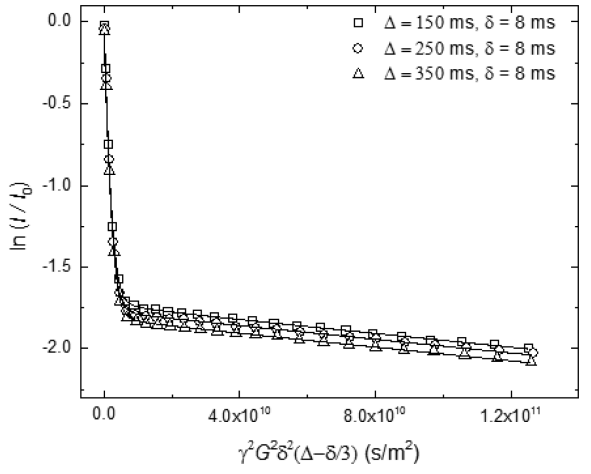

Figure 5. Experimental data and fitted echo curve of the proton from [EMIM] in the polymersome solution with various Δ. The data were fitted using eq 4.

polymersome solution gives two sets of resonances. The two resolved sets are attributed to the population of the ionic liquid inside and outside the polymersomes. The smaller set of peaks is slightly upfield and reflects [EMIM] in the vesicle interiors, as confirmed by comparing the experimental and theoretical mole fractions of [EMIM] in the interior and observing the relative intensity by changing the concentration of the polymersomes from 0.5 to 1.5 wt %. The values from the ^{1}H NMR spectra and from the theoretical calculation are consistent. The integrated fraction of the smaller peaks in the NMR is 0.21, and the mole fraction of the interior ionic liquid is 0.16. The theoretical mole fraction of the IL was calculated by using the solubility of [EMIM] in water (1.8 wt %) and the total volume fraction of the interior (estimated to be about 0.3%, based on the hydrodynamic radius and membrane thickness in this study). As shown in Figure S3, as the polymersome concentration increases, the fraction of smaller peaks also increases; this comparison clearly shows that satellite peaks are from the polymersome interiors. This chemical shift from the interiors was also observed for 1-butylimidazole (see Figure 6a) and [BMIM] (see Figure S4), which have diazole structures in common. The chemical shift is directly related to the magnetic field strength, which is a function of the magnetic susceptibility.[33] Since D_2O and [EMIM][TFSI] have different magnetic susceptibilities, the tracer molecules in this study showed two sets of peaks. Similar magnetic susceptibility effects on chemical shifts have also been found in the case of suspensions of red blood cells and emulsion systems.[33,34]

While [EMIM] was initially loaded into the polymersomes, 1-butylimidazole and [BMIM]Cl were added to the dispersion in the aqueous solution; both 1-butylimidazole and [BMIM] also showed additional sets of peaks after reaching equilibrium. This result directly demonstrates the permeation of tracer molecules through the membranes and also provides information on the population of the molecules in the interiors at equilibrium. If there was no permeation of the molecules, only a single set of peaks, from the exterior, should be evident in the spectra. By comparing the integrated areas of the free and confined peaks, the kinetics of permeation could potentially be monitored. After adding 50 mM of [BMIM]Cl to the polymersome solution, the integration of peaks for the exterior and interior molecules was monitored every 30 s. The transient results in Figure S5 show that the integrations do not change

dx.doi.org/10.1021/jp505118h | J. Phys. Chem. C 2014, 118, 21140−21147

Table 2. Permeation Rate with Two-Site Exchange Model

diffuser	D_e (m^2/s)	D_i (m^2/s)	P_i	P_e	$1/\tau_i$ (1/s)	$1/\tau_e$ (1/s)
[EMIM]	7.8×10^{-10}	2.1×10^{-12}	0.20	0.80	0.17	0.04
1-butylimidazole	5.8×10^{-10}	2.2×10^{-12}	0.07	0.93	2.5	0.18

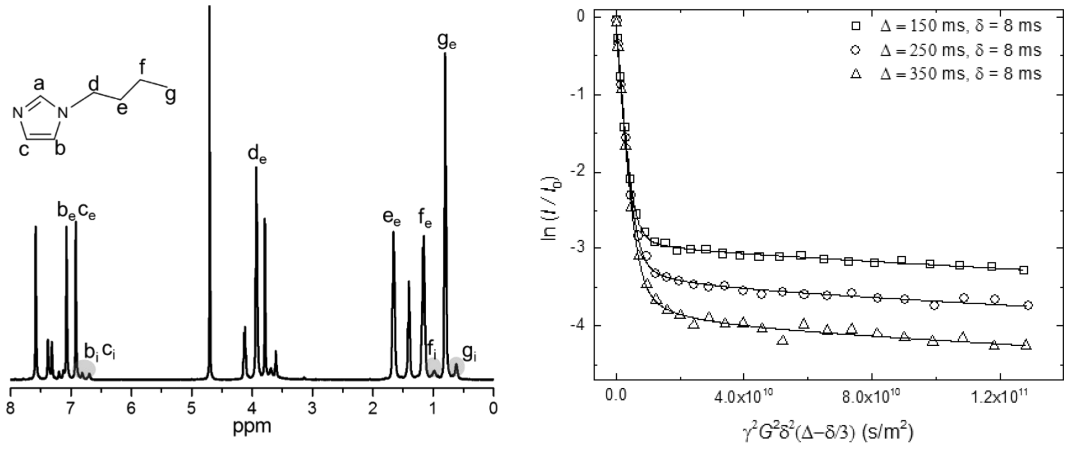

Figure 6. (a) ^{1}H NMR spectrum of 1-butylimidazole with BO(9−3) polymersomes. (b) Experimental data and fitted echo curves of the protons from 1-butylimidazole with various Δ. The data were fitted using eq 4.

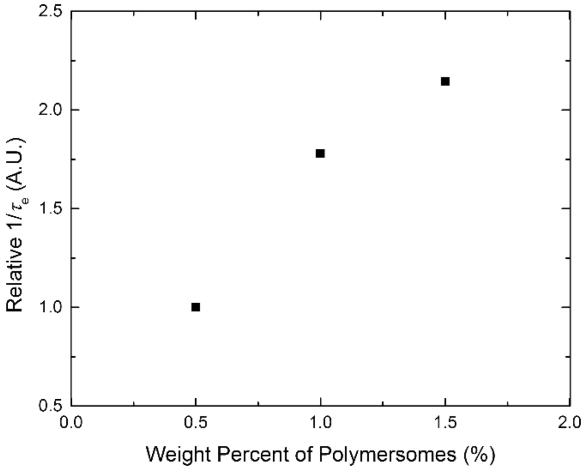

Figure 7. Relative rate of entry of 1-butylimidazole by changing the concentration of polymersome in the solution from 0.5 to 1.5 wt %. As the number of polymersomes increases, the rate of entry also increases.

with time. This indicates that even the charged [BMIM] molecules permeated through the hydrophobic PB membranes in well under 70 s. Kinetics at shorter times than 70 s could not be observed because at least a minute was needed for the addition of [BMIM]Cl, NMR tube injection, and shimming and locking.

Self-Diffusion of [EMIM] in D_2O and [EMIM][TFSI]. If there is no geometrical restriction for diffusion, the attenuated intensity of an individual tracer should follow eq 1, and the logarithm of normalized data points fall on a straight line with different diffusion times (Δ), as shown in Figure 3. The translation diffusion coefficient can be obtained from the slope. Figure 3 is the echo decay curve of [EMIM] in D_2O ([EMIM][TFSI] saturated) and in [EMIM][TFSI] (D_2O saturated). The solid lines are fits to eq 1; the diffusion coefficient (D) of [EMIM] in D_2O is 7.9×10^{-10} m^2/s and 7.9×10^{-11} m^2/s in [EMIM][TFSI]. These two values are close to the literature values.[35−37] According to the Stokes−Einstein equation ($D_{SE} = k_BT/(6\pi\eta R)$, where k_B is Boltzmann constant, T is the absolute temperature, η is the viscosity of a solvent, and R is the hydrodynamic radius), the diffusivity of objects should be proportional to the inverse of the solvent viscosity. However, in this case, this expectation is not realized. The viscosities of D_2O and [EMIM][TFSI] at 25 °C are 1.1 and 30.4 mPa·s, respectively, so the ratio of the inverse viscosities ($\eta_{[EMIM][TFSI]}/\eta_{heavy\ water}$) is around 28. In contrast, the ratio of the diffusivities for [EMIM] in water to that in the IL is around 10. This breakdown of this relation could be caused by several reasons. The calculated van der Waals radius of [EMIM] is 3 Å using the Hyperchem program.[38] Using the van der Waals radius as the hydrodynamic radius of [EMIM], the calculated D_{SE} values are 2.4×10^{-11} m^2/s in the IL and 6.5×10^{-10} m^2/s in D_2O. The actual diffusivity of [EMIM] is therefore greater in the IL but slower in D_2O than the values of D_{SE}. When a large spherical particle moves randomly in a continuous and viscous solvent without specific interactions, such as hydrogen bonding, the motion of the particle follows the Stokes−Einstein relation.[39] However, in the IL, the size of [EMIM] is similar to that of the dissociated [EMIM] or [TFSI] and smaller than the associated [EMIM][TFSI]. In general, for neutral molecules, the diffusivity of small solutes is enhanced relative to D_{SE} as the size ratio of solute to solvent molecules decreases.[40,42] Even though [EMIM] in the IL can associate and dissociate with its counterion,[36] [EMIM] showed an increased diffusivity due to the reduced friction as reported by Watanabe and Maroncelli groups.[35,36,43] These results are consistent with that of Edward.[40] In water, however, there are strong hydrogen bonding interactions between [EMIM] and water, which could reduce the diffusion coefficient.[37,44,45] The proton H_a is a good hydrogen bond donor, and there can be weak hydrogen bonding interaction between water and the protons of alkyl groups of [EMIM]. Nevertheless, the self-diffusion of [EMIM] in two saturated solutions suggests that the diffusion behavior is

dx.doi.org/10.1021/jp505118h | J. Phys. Chem. C 2014, 118, 21140−21147

largely dictated by viscosity of diffusion medium. In addition, with a single set of distinct peaks of [EMIM] protons in the NMR spectra, the single-exponential echo decays in each phase imply that the ionic liquid and D_2O do not form long-lived aggregates in D_2O and the ionic liquid, respectively.

Escape and Entry Rates of [EMIM] and 1-Butylimidazole. Diffusion of probe molecules in the polymersome solution is not the same as free diffusion, due to the restricted geometry, and thus cannot be simply described by eq 1. For short diffusion times, the behavior is still within the range of the free diffusion. But over time scales where the mean displacement of the molecule is comparable to the dimension of the restricted geometry, the translation of the molecule in the laboratory frame is affected by the random walks of both the moving vesicles and the tracer molecules.[46] In the long time limit, the diffusion behavior of the tracer molecules confined in the vesicles should be similar to that of the vesicles because the net displacement is much larger than the vesicle radius. For example, when an [EMIM] molecule and a vesicle (radius 100 nm) move with $D_{[EMIM]} = 1 \times 10^{-9}$ m^2/s and $D_{vesicle} = 1 \times 10^{-12}$ m^2/s by three-dimensional random walks in water, the mean displacements, s, during the observation time, t (e.g., 100 ms), are about 25 and 0.8 μm, respectively, according to Einstein's relationship, $s = (6Dt)^{0.5}$. Since the mean displacement of the tracer molecule is 2 orders of magnitude larger than the radius of the polymersomes, the diffusion of molecules is restricted within the confined vesicles and should have a similar displacement to the moving vesicle (see Figure 4).[22] Moreover, the molecules in each site can be exchanged through the membranes. So the transmembrane exchange and the diffusion behavior should be described in a different way, and the two-site exchange approximation is a powerful tool to explain the exchange rate and the diffusion behavior.[47] In this model, exchange terms are added to Fick's second law of diffusion as shown in eqs 2 and 3

$$\frac{\partial C_i}{\partial t} = D_i \nabla^2 C_i - \frac{C_i}{\tau_i} + \frac{C_e}{\tau_e} \quad (2)$$

$$\frac{\partial C_e}{\partial t} = D_e \nabla^2 C_e - \frac{C_e}{\tau_e} + \frac{C_i}{\tau_i} \quad (3)$$

where C_i, D_i, and τ_i represent the concentration (mol/L), the diffusion coefficient (m^2/s), and residence time (s) of a tracer molecule in the interiors of polymersomes, respectively, and C_e, D_e, and τ_e, represent the same parameters in the external aqueous medium.

For the PFG-NMR experiment, the solution of eqs 2 and 3 is a biexponential function

$$\frac{I}{I_0} = P_a' \exp(-k_a'(\Delta - \delta/3)) + P_b' \exp(-k_b'(\Delta - \delta/3)) \quad (4)$$

where P_a', P_b', k_a', and k_b' are the apparent mole fraction of probe molecules and rate constants, which are functions of the real parameters, P_i, P_e, D_i, D_e, τ_i, and τ_e (see Supporting Information). P_i and P_e stand for the mole fraction of probe molecules in the encapsulated and free space ($P_i + P_e = 1$); τ_i and τ_e are the residence time at each phase, and the inverse of the residence times represents the rate of escape ($1/\tau_i$, path 1 in Figure 4) and entry ($1/\tau_e$, path 2 in Figure 4), respectively. The residence times are also related by $\tau_e = (1 - P_i) \times \tau_i/P_i$.

[EMIM] and 1-butylimidazole were employed as the tracer molecules for the PFG-NMR study. The gradient strength (G) was varied from 98% to 2% of the maximum gradient strength (0.47 T/m) for a duration δ = 8 ms. The NMR spectra of protons, H_b and H_c of [EMIM] and 1-butylimidazole (see Figure 2 for [EMIM] and Figure 6a for 1-butylimidazole), were recorded during three different diffusion times (Δ = 150, 250, and 350 ms). Since the exchange across the membranes occurs, both peaks from the interiors and the exteriors were integrated together through DOSY processing. The integrated results were fitted with the two-site model. Two apparent diffusion coefficients, D_i and D_e, were obtained from the initial and final slopes of the decay curves, and other parameters (Δ, δ, G, γ) were given. By the fitting, the residence time ($\tau_{i,e}$) and the mole fraction of the molecules in each site ($P_{i,e}$) can be obtained. Note that because the two residence times and the two populations are related, there are only two parameters in the fits, given that the two D's are set by the initial and final slopes. Also, the measurements were repeated several times to ensure the reliability of the fits. Finally, the values of ($P_{i,e}$) are also confirmed by the independent ^{1}H NMR spectra.

Figure 5 shows the experimental data (□, ○, △) and fitted echo decay curve (solid line) of H_b and H_c on [EMIM]. The fitted results are summarized in Table 2. P_i of [EMIM] is 0.2, which is very close to the mole fraction of [EMIM] in the polymersomes from the 1-D spectrum (Figure 2). The mean residence time of molecules in the inside of polymersomes is $\tau_i \approx 5.8$ s, and that in the exterior is $\tau_e \approx 23$ s. In the case of 1-butylimidazole, due to the similar chemical structure with [EMIM], many peaks are not distinguishable from the [EMIM] peaks. Apparently distinguishable peaks are assigned in Figure 6a. For PFG-NMR, H_b and H_c of 1-butylimidazole were also used, and the data (□, ○, △) and fit (solid line) are shown in Figure 6b. The parameters are also summarized in Table 2: $P_i \approx 0.07$, $\tau_i \approx 0.4$ s, and $\tau_e \approx 5.4$ s for 1-butylimidazole.

D_e and D_i represent the diffusion behavior of the molecules in the limit of short and long diffusion times, respectively. D_e values are similar to the free diffusion in D_2O, but the D_i values are somewhat lower than the diffusion coefficient of the vesicles from the DLS measurement, which was 3.0×10^{-12} m^2/s in D_2O. By using the Stokes–Einstein equation, R_h from NMR is 90 nm, which is bigger than that from the light scattering experiment (64 nm). This difference can be explained, at least in part, by the slower diffusion in a more concentrated solution. While the weight fraction of polymersomes was 0.01 wt % in the DLS measurement, the weight fraction in the NMR measurement was 0.5 wt %. The motion of the polymersomes in the concentrated solution can be retarded by the interaction between the vesicles.[48] Dispersity of vesicle size may also contribute to the small difference between NMR and DLS.

As the observation time (Δ) increases, the number of molecules that are initially observed in the confined interiors decreases because there are more exchanges of tracer molecules during the longer Δ.[49] The difference of plateaus of 1-butylimidazole is much bigger than that of [EMIM] (see Figures 5 and 6b). Since longer residence time means that molecules prefer to be in the initial site, it can be concluded that the charged [EMIM] was slower to exchange through the hydrophobic PB membranes than the neutral 1-butylimidazole. It is therefore apparent that the charged molecules are less exchangeable across the hydrophobic membranes. Permeability is defined as a product of solubility and diffusivity of a tracer molecule in a permeation medium.[50,51] For charged and neutral

dx.doi.org/10.1021/jp505118h | J. Phys. Chem. C 2014, 118, 21140–21147

molecules of similar size, the diffusivity should not be very different.[52] But charged molecules experience a higher barrier to dissolve in hydrophobic membrane, reflected in a higher partitioning difference.[53] Hence, the difference of permeation rate of the two tracer molecules arises primarily from the solubility difference in the PB membranes. Note that even if the charged molecule diffuses through the membrane as an ion pair, that would only reduce the diffusivity by a factor of about 2. The speed of escape ($1/\tau_i$) and entry ($1/\tau_e$) were also evaluated. The higher rate means higher permeation. Both $1/\tau_i$ and $1/\tau_e$ of 1-butylimidazole are an order of magnitude higher than that of [EMIM], as expected from the decay curve appearance.

Furthermore, the effect of the polymersome concentration on the rate of entry ($1/\tau_e$) was studied. Three solutions having different concentrations were prepared, and PFG-NMR was conducted with same concentration of 1-butylimidazole (50 mM). P and τ values were obtained by fitting with the two-site exchange model. As shown in Figure 7, as the polymersome content increases, $1/\tau_e$ increases. With increasing the number of polymersomes, the total surface area for permeation also increases. Higher number of polymersomes provided more surface area to the diffusing molecules, and they had more probability to penetrate through the membranes. This result coincides with the study of the vesicle size effect on the permeation rate. As the size of vesicle decreased, the molecular exchange rate increased because the membrane surface to the vesicle volume ratio increased with decreasing vesicle size.[54]

SUMMARY

Polymersomes of BO(9−3) with [EMIM][TFSI] interiors dispersed in water were created by transferring the polymersomes in prepared [EMIM][TFSI] to water. The permeation of various tracer molecules through the membranes in this nanoemulsion solution was investigated by NMR techniques. Because of the magnetic susceptibility difference across the membrane, the permeation of [BMIM] and 1-butylimidazole was easily confirmed in 1-D ^{1}H NMR spectra. Moreover, the mole fraction of the tracer molecules in the interiors could be calculated by integrating of each set of peaks. PFG-NMR was also employed to investigate the speed of escape and entry of two similarly sized tracer molecules having different charges. The charged [EMIM] and the neutral 1-butylimidazole were permeable through the hydrophobic PB membranes with reasonable speed, but the rate of permeation of the neutral molecules was greater than the charged ones, in both directions. This permeation study by using NMR about the rate of molecular transportation across the polymersome membrane will inform the design of a nanoreactor system based on the polymersomes with IL interiors in water.

ASSOCIATED CONTENT

Supporting Information

DLS results of the polymersomes in [EMIM][TFSI], the cryo-TEM image of the polymersomes with [EMIM][TFSI] in water, normalized ^{1}H NMR spectra of polymersome solutions (0.5, 1.0, and 1.5 wt %), chemical structure of [BMIM], ^{1}H NMR spectrum of [BMIM] solution with BO(9−3) polymersome, the result of the kinetic experiment with [BMIM], and details of two-site exchange model. This material is available free of charge via the Internet at http://pubs.acs.org.

AUTHOR INFORMATION

Corresponding Author

*E-mail: lodge@umn.edu (T.P.L.).

Notes

The authors declare no competing financial interest.

ACKNOWLEDGMENTS

This work was supported by the National Science Foundation through Award DMR-1206459. Cryo-TEM measurements were carried out in the CSE Characterization Facility, University of Minnesota, which receives partial support from the NSF through the MRSEC program. We acknowledge Dr. Megan L. Hoarfrost for helpful discussions and Dr. Letitia Yao for help with the NMR measurements.

REFERENCES

(1) Lee, J. C. M.; Bermudez, H.; Discher, B. M.; Sheehan, M. A.; Won, Y. Y.; Bates, F. S.; Discher, D. E. Preparation, Stability, and In Vitro Performance of Vesicles Made with Diblock Copolymers. *Biotechnol. Bioeng.* **2001**, *73*, 135−145.

(2) Meng, F.; Zhong, Z.; Feijen, J. Stimuli-Responsive Polymersomes for Programmed Drug Delivery. *Biomacromolecules* **2009**, *10*, 197−209.

(3) Watanabe, K.; Takizawa, S.-Y.; Murata, S. Hydrogen Generation Using a Photoinduced Electron-transport System with a Molecular Catalyst in Vesicles. *Chem. Lett.* **2011**, *40*, 345−347.

(4) Yow, H. N.; Routh, A. F. Formation of Liquid Core-Polymer Shell Microcapsules. *Soft Matter* **2006**, *2*, 940−949.

(5) Renggli, K.; Baumann, P.; Langowska, K.; Onaca, O.; Bruns, N.; Meier, W. Selective and Responsive Nanoreactors. *Adv. Funct. Mater.* **2011**, *21*, 1241−1259.

(6) Discher, D. E.; Eisenberg, A. Polymer Vesicles. *Science* **2002**, *297*, 967−973.

(7) Bai, Z.; Lodge, T. P. Polymersomes with Ionic Liquid Interiors Dispersed in Water. *J. Am. Chem. Soc.* **2010**, *132*, 16265−16270.

(8) Yu, S.; Azzam, T.; Rouiller, I.; Eisenberg, A. "Breathing" Vesicles. *J. Am. Chem. Soc.* **2009**, *131*, 10557−10566.

(9) Kim, K. T.; Meeuwissen, S. A.; Nolte, R. J. M.; van Hest, J. C. M. Smart Nanocontainers and Nanoreactors. *Nanoscale* **2010**, *2*, 844−858.

(10) Palivan, C. G.; Fischer-Onaca, O.; Delcea, M.; Itel, F.; Meier, W. Protein−Polymer Nanoreactors for Medical Applications. *Chem. Soc. Rev.* **2012**, *41*, 2800−2823.

(11) Bai, Z.; Lodge, T. P. Thermodynamics and Mechanism of the Block Copolymer Micelle Shuttle Between Water and an Ionic Liquid. *J. Phys. Chem. B* **2009**, *113*, 14151−14157.

(12) Loverdo, C.; Benichou, O.; Moreau, M.; Voituriez, R. Enhanced Reaction Kinetics in Biological Cells. *Nat. Phys.* **2008**, *4*, 134−137.

(13) Sato, T.; Kijima, M.; Shiga, Y.; Yonezawa, Y. Photochemically Controlled Ion Permeability of Liposomal Membranes Containing Amphiphilic Azobenzene. *Langmuir* **1991**, *7*, 2330−2335.

(14) Wu, J.; Eisenberg, A. Proton Diffusion Across Membranes of Vesicles of Poly(styrene-*b*-acrylic acid) Diblock Copolymers. *J. Am. Chem. Soc.* **2006**, *128*, 2880−2884.

(15) Rodríguez-García, R.; Mell, M.; López-Montero, I.; Netzel, J.; Hellweg, T.; Monroy, F. Polymersomes: Smart Vesicles of Tunable Rigidity and Permeability. *Soft Matter* **2011**, *7*, 1532−1542.

(16) Paula, S.; Volkov, A. G.; Deamer, D. W. Permeation of Halide Anions through Phospholipid Bilayers Occurs by the Solubility-Diffusion Mechanism. *Biophys. J.* **1998**, *74*, 319−327.

(17) Bolinger, P.; Stamou, D.; Vogel, H. Integrated Nanoreactor Systems: Triggering the Release and Mixing of Compounds Inside Single Vesicles. *J. Am. Chem. Soc.* **2004**, *126*, 8594−8595.

(18) Bai, Z.; Zhao, B.; Lodge, T. P. Bilayer Membrane Permeability of Ionic Liquid-filled Block Copolymer Vesicles in Aqueous Solution. *J. Phys. Chem. B* **2012**, *116*, 8282−8289.

(19) Battaglia, G.; Ryan, A. J.; Tomas, S. Polymeric Vesicle Permeability: A Facile Chemical Assay. *Langmuir* **2006**, *22*, 4910−4913.
(20) Choudhury, R. P.; Galvosas, P.; Schönhoff, M. Scaling Law of Poly(ethylene oxide) Chain Permeation through a Nanoporous Wall. *J. Phys. Chem. B* **2008**, *112*, 13245−13251.
(21) Clarke, R. J.; Apell, H.-J. A Stopped-flow Kinetic Study of the Interaction of Potential-Sensitive Oxonol Dyes with Lipid Vesicles. *Biophys. Chem.* **1989**, *34*, 225−237.
(22) Price, W. S. Pulsed-field Gradient Nuclear Magnetic Resonance as a Tool for Studying Translational Diffusion: Part 1. Basic Theory. *Concepts Magn. Reson.* **1997**, *9*, 299−336.
(23) Rumplecker, A.; Föster, S.; Zähres, M.; Mayer, C. Molecular Exchange through Vesicle Membranes: A Pulsed Field Gradient Nuclear Magnetic Resonance Study. *J. Chem. Phys.* **2004**, *120*, 8740−8747.
(24) Wong, B.; Boyer, C.; Steinbeck, C.; Peters, D.; Schmidt, J.; Zanten, R.; Chmelka, B.; Zasadzinski, J. Design and In Situ Characterization of Lipid Containers with Enhanced Drug Retention. *Adv. Mater.* **2011**, *23*, 2320−2325.
(25) Meli, L.; Santiago, J. M.; Lodge, T. P. Path-Dependent Morphology and Relaxation Kinetics of Highly Amphiphilic Diblock Copolymer Micelles in Ionic Liquids. *Macromolecules* **2010**, *43*, 2018−2027.
(26) Freire, M. G.; Carvalho, P. J.; Gardas, R. L.; Marrucho, I. M.; Santos, L. M. N. B. F.; Coutinho, J. A. P. Mutual Solubilities of Water and the $[C_n mim][Tf_2N]$ Hydrophobic Ionic Liquids. *J. Phys. Chem. B* **2008**, *112*, 1604−1610.
(27) Wu, D.; Chen, A.; Johnson, C. S. An Improved Diffusion-Ordered Spectroscopy Experiment Incorporating Bipolar-Gradient Pulses. *J. Magn. Reson.* **1995**, *115*, 260−264.
(28) Jakes, J. Regularized Positive Exponential Sum (REPES) Program - A Way of Inverting Laplace Transform Data Obtained by Dynamic Light Scattering. *Collect. Czech. Chem. Commun.* **1995**, *60*, 1781−1797.
(29) He, Y.; Li, Z.; Simone, P. M.; Lodge, T. P. Self-Assembly of Block Copolymer Micelles in an Ionic Liquid. *J. Am. Chem. Soc.* **2006**, *128*, 2745−2750.
(30) Simone, P. M.; Lodge, T. P. Lyotropic Phase Behavior of Polybutadiene-Poly(ethylene oxide) Block Copolymers in Ionic Liquids. *Macromolecules* **2008**, *41*, 1753−1759.
(31) Davis, K.; Lodge, T. P.; Bates, F. S. Vesicle Membrane Thickness in Aqueous Dispersions of Block Copolymer Blends. *Macromolecules* **2008**, *41*, 8289−8291.
(32) Hesse-Ertelt, S.; Heinze, T.; Kosan, B.; Schwikal, K.; Meister, F. Solvent Effects on the NMR Chemical Shifts of Imidazolium-Based Ionic Liquids and Cellulose Therein. *Macromol. Symp.* **2010**, *294*, 75−89.
(33) Kuchel, P. W.; Chapman, B. E.; Bubb, W. A.; Hansen, P. E.; Durrant, C. J.; Hertzberg, M. P. Magnetic Susceptibility: Solutions, Emulsions, and Cells. *Concepts Magn. Reson.* **2003**, *18A*, 56−71.
(34) Skibsted, U.; Hansen, P. E. ^{1}H NMR Spin-Echo Spectroscopy of Human Erythrocytes. Transformation of Exogenous Compounds. *NMR Biomed.* **1990**, *3*, 248−258.
(35) Noda, A.; Hayamizu, K.; Watanabe, M. Pulsed-Gradient Spin-Echo ^{1}H and ^{19}F NMR Ionic Diffusion Coefficient, Viscosity, and Ionic Conductivity of Non-chloroaluminate Room-Temperature Ionic Liquids. *J. Phys. Chem. B* **2001**, *105*, 4603−4610.
(36) Tokuda, H.; Tsuzuki, S.; Susan, Md.; Hayamizu, K.; Watanabe, M. How Ionic Are Room-Temperature Ionic Liquids? An Indicator of the Physicochemical Properties. *J. Phys. Chem. B* **2006**, *110*, 19593−19600.
(37) Sarraute, S.; Gomes, M.; Pádua, A. Diffusion Coefficients of 1-Alkyl-3-methylimidazolium Ionic Liquids in Water, Methanol, and Acetonitrile at Infinite Dilution. *J. Chem. Eng. Data* **2009**, *54*, 2389−2394.
(38) McEwen, A. B.; Ngo, H. L.; LeCompte, K.; Goldman, J. L. Electrochemical Properties of Imidazolium Salt Electrolyte for Electrochemical Capacitor Applications. *J. Electrochem. Soc.* **1999**, *146*, 1687−1695.
(39) Geyer, U.; Johnson, W. L.; Schneider, S.; Qiu, Y.; Tombrello, T. A.; Macht, M.-P. Small Atom Diffusion and Breakdown of the Stokes-Einstein Relation in the Supercooled Liquid State of the $Zr_{46.7}Ti_{8.3}Cu_{7.5}Ni_{10}Be_{27.5}$ Alloy. *Appl. Phys. Lett.* **1996**, *69*, 2492−2494.
(40) Edward, J. T. Molecular Volumes and the Stokes-Einstein Equation. *J. Chem. Educ.* **1970**, *47*, 261−270.
(41) Sharman, M.; Yashonath, S. Size Dependence of Solute Diffusivity and Stokes-Einstein Relationship: Effect of van der Waals Interaction. *Diffus. Fundam.* **2007**, *7*, 11.1−11.15.
(42) Bhattacharyya, S.; Bagchi, B. Anomalous Diffusion of Small Particles in Dense Liquids. *J. Chem. Phys.* **1997**, *106*, 1757−1763.
(43) Kaintz, A.; Baker, G.; Benesi, A.; Maroncelli, M. Solute Diffusion in Ionic Liquids, NMR Measurements and Comparisons to Conventional Solvents. *J. Phys. Chem. B* **2013**, *117*, 11697−11708.
(44) Gonfa, G.; Bustam, M. A.; Man, Z.; Abdul Mutalib, M. I. Unique Structure and Solute-Solvent Interaction in Imidazolium Based Ionic Liquids: A Review. *Asian Trans. Eng.* **2011**, *1*, 24−34.
(45) Zhang, Q.; Wang, N.; Yu, Z. The Hydrogen Bonding Interactions Between the Ionic Liquid 1-Ethyl-3-methylimidazolium Ethyl Sulfate and Water. *J. Phys. Chem. B* **2010**, *114*, 4747−4754.
(46) Ochab-Marcinek, A.; Hołyst, R. Scale-Dependent Diffusion of Spheres in Solutions of Flexible and Rigid Polymers: Mean Square Displacement and Autocorrelation Function for FCS and DLS Measurements. *Soft Matter* **2011**, *7*, 7366−7374.
(47) Kärger, J. NMR Self-Diffusion Studies in Heterogeneous Systems. *Adv. Colloid Interface Sci.* **1985**, *23*, 129−148.
(48) Adalsteinsson, T.; Dong, W.; Schönhoff, M. Diffusion of 77000 g/mol Dextran in Submicron Polyelectrolyte Capsule Dispersions Measured Using PFG-NMR. *J. Chem. Phys.* **2004**, *108*, 20056−20063.
(49) Linders, J.; Mayer, C.; Sekine, T.; Hoffmann, H. Pulsed-Field Gradient NMR Measurements on Hydrogels from Phosphocholine. *J. Chem. Phys.* **2012**, *116*, 11459−11465.
(50) Krevelen, D. W. *Properties of Polymers*, 4th ed.; Elsevier: Solvonia, 2009.
(51) Wijmans, J. G.; Baker, R. W. The Solution-Diffusion Model: A Review. *J. Membr. Sci.* **1995**, *107*, 1−21.
(52) Kisak, E. T.; Coldren, B.; Evans, C. A.; Boyer, C.; Zasadzinski, J. A. The Vesosome - A Multicompartment Drug Delivery Vehicle. *Curr. Med. Chem.* **2004**, *11*, 199−219.
(53) Paula, S.; Volkov, A. G.; Deamer, D. W. Permeation of Halide Anions through Phospholipid Bilayers Occurs by the Solubility-Diffusion Mechanism. *Biophys. J.* **1998**, *74*, 319−327.
(54) Leson, A.; Leson, A.; Hauschild, S.; Rank, A.; Neub, A.; Schubert, R.; Forster, S.; Mayer, C. Molecular Exchange Through Membranes of Poly(2-vinylpyridine-*block*-ethylene oxide) Vesicles. *Small* **2007**, *3*, 1074−1083.